Journal of Marine Research, 54, 211–238, 1996

On frontal and ventilated models of the main thermocline

by Simon Hood[1] and Richard G. Williams[1]

ABSTRACT

A new similarity approach is applied to the thermocline equations in order to examine contrasting frontal and ventilated models of the main thermocline. The method of solution involves reducing the number of independent variables of the controlling partial differential equation, leading to a particular form for the solutions which satisfy appropriate boundary conditions.

A frontal model of the thermocline is obtained following the study of Salmon and Hollerbach (1991). When the vertical diffusivity becomes vanishingly small, an interior front in the subtropical gyre appears at the depth where the vertical velocity changes sign. The front separates downwelling warm water in the subtropical gyre from the underlying upwelling of cold, deep water. These solutions appear to be robust to changes in the vertical diffusivity profile, as long as there is a small, nonzero value in the interior. However, when there is uniform diffusivity, there is no implied surface heat flux and surface isotherms are coincident with streamlines. As the diffusivity increases toward the surface, the surface heat input increases in magnitude and the temperature field becomes more plausible.

A ventilated model of the thermocline is formed using the similarity approach with a diffusive surface boundary-layer overlying an adiabatic interior. In this case, the temperature and velocity fields are solved for in the limit of uniform potential vorticity. There is now a more plausible cross-isothermal flow in the surface layer with a polewards decrease in temperature, and the implied surface heat input increases equatorwards. Fluid is subducted from the surface boundary layer into the adiabatic interior and forms a continuous thermocline.

In conclusion, the contrasting frontal and ventilated solutions arise from modeling different aspects of the circulation, rather than depending on the type of model employed. The ventilated solutions form a thermocline by advecting the surface temperature field into the interior of a subtropical gyre, whereas the frontal solutions create a thermocline from the interaction of the wind-driven gyre and the underlying thermohaline circulation. These thermocline solutions might occur separately or together in the real ocean, although both solutions might be modified by higher-order processes or more complicated forcing.

1. Introduction

A striking feature throughout the ocean is a persistent thermocline with a large vertical temperature gradient over the upper 1 km, which overlies relatively homogeneous, deeper water. Explaining the presence of the thermocline requires solving the

1. Oceanography Laboratories, University of Liverpool, Liverpool, United Kingdom, L69 3BX.

steady, thermodynamic equation:

$$\boldsymbol{u} \cdot \nabla\theta = \boldsymbol{B}. \tag{1.1}$$

The thermodynamic equation, (1.1), is nonlinear, as the temperature field θ influences the velocity field, $\boldsymbol{u}$, through the thermal-wind balance; here, $\boldsymbol{B}$ represents the thermodynamic forcing. Consequently, solution of this problem is not trivial and has been examined for some time—see reviews of previous work by Pedlosky (1986) and Rhines (1986).

Early thermocline work used a similarity approach with a continuous stratification and advocated two opposing limits: diffusive control by Robinson and Stommel (1959) and advective control by Welander (1959). However, these and subsequent similarity solutions have been criticized in being over complex and unable to satisfy general boundary conditions.

Recent theoretical studies have employed simplified layered models designed to focus on the controlling physical processes in the advective limit. Rhines and Young (1982) (henceforth RY) have emphasized the role of geostrophic eddies in homogenizing properties over ocean gyres using a quasi-geostrophic model. Luyten *et al.* (1983) (henceforth LPS) have instead argued for the ventilated control of the thermocline using a layered model over the interior of the subtropical gyre. However, neither of these simplified models provide a complete representation of the global ocean, as the thermohaline circulation is not properly included with RY imposing the background stratification and LPS only solving for a thermocline over a motionless abyss.

In contrast, Salmon (1990), using numerical experiments, and Salmon and Hollerbach (1991) (henceforth SH), using a similarity approach, argue that the main thermocline is an internal front. In the limit of vanishingly small vertical diffusivity, the front appears as an internal boundary layer over the subtropical gyre, but not over the subpolar gyre. The front is located at the depth where the vertical velocity w vanishes and changes sign. The front results from the downwelling of warm, surface water meeting the upwelling of cold, deep water; hence, it is due to the interaction of the wind-driven gyre and the underlying thermohaline circulation. However, these solutions are unrealistic in showing no implied surface heat flux and surface isotherms coincident with streamlines, rather than there being a more plausible poleward decrease in surface temperature.

Each of these theoretical models have different attributes, but understanding the crucial differences in them has been hampered through the contrasting choices in model formulation. In this study, we examine the LPS and SH limits using the same similarity approach to solve the thermocline equations over a subtropical gyre away from the lateral boundaries. Firstly, we discuss in more detail the physical assumptions made in the LPS and SH models, and secondly we describe the rationale for this work.

LPS solve for the structure of the main thermocline using a layered model after

imposing the Ekman pumping and the surface temperature field. The main thermocline results from the surface temperature field being advected into the interior by the circulation induced by Ekman pumping in a subtropical gyre. The flow is assumed to be adiabatic in the interior with streamlines coincident with isotherms, i.e.,

$$u\theta_x + v\theta_y + w\theta_z = 0, \tag{1.2}$$

here u, v and w are the velocities in the x, y and z directions. The LPS solutions require an implicit surface boundary layer, which is included in the mixed-layer extensions by Pedlosky *et al.* (1984) and Williams (1989). Over a vertically-homogeneous mixed layer, (1.1) becomes

$$u\theta_x + v\theta_y = \frac{\mathscr{H}}{\rho C_p h}; \tag{1.3}$$

here $\mathscr{H}$ is the surface heat flux, h is the mixed-layer depth, ρ is a reference density and C_p is the heat capacity. The diabatic forcing drives a cross-isothermal flow in the surface boundary layer and subduction of fluid from the mixed layer into the underlying thermocline; subduction ceases in the limit of no heat being supplied to the geostrophic flow in the mixed layer (see Nurser and Marshall, 1991).

Salmon (1990) recently cast doubt on the LPS solutions arguing that the surface temperature field should be solved for rather than imposed. Accordingly, SH employ a similarity approach to solve for the entire flow field and temperature field. The thermodynamic forcing is simply represented by a vertical diffusion of heat with a constant diffusivity, κ, i.e.,

$$u\theta_x + v\theta_y + w\theta_z = \kappa\theta_{zz}. \tag{1.4}$$

In the limit of vanishing diffusivity, an internal front is found to appear in the subtropical gyre where w changes sign, which SH interprets as the main thermocline.

In this study we examine the contrasting frontal and ventilated models of the main thermocline in an idealized subtropical gyre with uniform Ekman pumping. The sensitivity of the solutions to different choices in the vertical velocity and diffusivity profiles is examined. Following SH, we parameterize the diabatic forcing in terms of a vertical diffusion of heat, but allow the vertical diffusivity to vary in the vertical. This leads to the modified thermodynamic equation

$$u\theta_x + v\theta_y + w\theta_z = (\kappa\theta_z)_z. \tag{1.5}$$

The right-hand side may be interpreted in terms of a vertical divergence of a heat flux (cf. 1.3) with the heat flux given by

$$\mathscr{H} = \rho C_p \kappa \theta_z. \tag{1.6}$$

The diffusivity profile is allowed to range from a constant value throughout the domain to a spatially-varying case with large κ at the surface and zero value in the

interior. Our choices in diffusivity are stimulated by the observed bias in the diabatic forcing over the ocean. The surface heat fluxes into the seasonal boundary layer reach the order of 100 W m^{-2}, whereas the diffusive heat fluxes are several orders of magnitude smaller in the ocean interior. Likewise, the turbulent mixing reaches the order of 10^{-3} W m^{-3} in the surface convection layer, whereas it decreases to 10^{-6} W m^{-3} in the thermocline (see review by Woods, 1984).

The paper is structured in the following way. The controlling thermocline equations, model domain and boundary conditions for an idealized subtropical gyre are described in Section 2. New thermocline solutions for the frontal and ventilated limits are obtained using a similarity approach in Sections 3 and 4; the method is less restrictive than that employed by SH and is fully described in the companion paper by Hood (1996)—hereafter 'Paper I'. The sensitivity of these thermocline solutions is examined by modifying the vertical velocity boundary conditions and the diffusivity profile. Finally the main results are discussed in Section 5.

2. The thermocline equations

The controlling thermocline equations may be written in nondimensional form as

$$fu = -P_y, \qquad fv = P_x, \qquad \theta = P_z, \tag{2.1a}$$

$$u_x + v_y + w_z = 0, \tag{2.1b}$$

$$u\theta_x + v\theta_y + w\theta_z = (\kappa\theta_z)_z, \tag{2.1c}$$

where P is pressure and $f = y$ is the Coriolis parameter. These equations are used to model the steady, gyre-scale flow away from lateral boundaries; time dependence, inertia, friction and temperature diffusion in the horizontal are neglected. Following Welander (1959) and SH, we define a "potential," $M(x, y, z)$, to satisfy

$$u = -\frac{1}{y}M_{yz}, \qquad v = \frac{1}{y}M_{xz}, \qquad w = \frac{1}{y^2}M_x, \tag{2.2i}$$

$$P = M_z, \qquad \theta = M_{zz} \tag{2.2ii}$$

and then with no loss of generality (2.1) are represented by the single equation for the thermodynamic equation:

$$M_x M_{zzz} + y(M_{xz}M_{yzz} - M_{yz}M_{xzz}) = y^2(\kappa_z M_{zzz} + \kappa M_{zzzz}). \tag{2.3}$$

The advection of heat is represented by the left-hand side of the equation (in the order of $w\theta_z$, $v\theta_z$ and $u\theta_z$) and the vertical diffusion of heat by the right-hand side ($\kappa_z\theta_z$ and $\kappa\theta_{zz}$). Note that the first term on the right-hand side vanishes when κ is uniform, as assumed by SH. For future reference, also note that potential vorticity, q, is given by

$$q = y\theta_z = yM_{zzz}. \tag{2.4}$$

From (2.3) it is easy to see that we have the freedom to translate both x and z, and freedom to rescale x, y and z (by rescaling M if necessary). Therefore, since $y = 0$ corresponds to the equator, we may consider the solution domain

$$(x, y, z) \in [0, 1]^3, \tag{2.5}$$

without loss of generality; to see this formally, consider transformations $\boldsymbol{v}_1$, $\boldsymbol{v}_2$, $\boldsymbol{v}_3$, $\boldsymbol{v}_4$, and $\boldsymbol{v}_5$ in Table 1 of SH.

We consider an idealized subtropical gyre and solve for the flow below the surface Ekman layer. The following boundary conditions are applied:

(i) vertical velocity decreases to zero in the deep ocean, i.e., $w \to 0$ as $z \to 0$ (although this condition is relaxed in one of our frontal cases);

(ii) there is a uniform Ekman pumping at the base of the surface Ekman layer, i.e., $w = w_E$ at $z = 1$.

In reality, the Ekman pumping should vary in space and define the domain of the subtropical gyre. However, we have simplified the forcing so as to focus on the role of the diabatic forcing; consequently, the solutions close to the equator are not physically relevant, as there should be different dynamical balances there.

(iii) There is no net flow through the entire eastern boundary, i.e.,

$$\int_0^1 \int_0^1 u(x = 1, y, z) dy dz = 0. \tag{2.6}$$

Note that (iii) is a weaker constraint than that used by SH who impose the condition of no depth-integrated flow at all latitudes, i.e., $\int u(x = 1, y, z)\, dz = 0$. The western, northern and southern boundaries are assumed to be passive and supply whatever volume flux is required by the interior; this assumption is frequently applied in thermocline models.

Neither the surface temperature or surface heat flux are imposed as explicit boundary conditions, but instead are solved for according to the pattern of flow and form of diabatic forcing. However, the heat flux through the sea floor is always set to zero. A family of solutions may satisfy these applied boundary conditions. Our approach is to show how the character of these thermocline solutions changes according to different physical assumptions, rather than try to isolate a definitive solution for the real ocean.

3. Frontal solutions

In this section the frontal model of the thermocline advocated by SH is examined using new similarity-based solutions obtained in Paper I. The sensitivity of the frontal solutions is examined to different choices in the vertical velocity boundary conditions and the diffusivity profile.

Our similarity approach to determining solutions of (2.3) follows that of Clarkson and Kruskal (1989) and is more general than the method, due to Lie, used by SH, though it is also based on the use of *symmetry reductions.*[2] The essential idea is to find a transformation which reduces the number of independent variables in (2.3) from three to two which, at least in principle, simplifies the problem of solution. Generality of solution is lost, but experience suggests that physical solutions are still retained. The details of computation of such transformations are presented in Paper I and we simply quote the results here. In this paper we consider solution of the *reduced equation* (see Section 1, Paper I) and application of the results.

a. Frontal solutions of Salmon and Hollerbach

In this section we recover the main results obtained by SH by choosing diffusivity, κ, to be uniform and applying a Reduction computed in Paper I; this is extended in the following sections. We also demonstrate that the method used here is more general than that applied by SH.

First, recall Reduction 3.2.4, from Paper I, in which the potential, $M(x, y, z)$ is given by

$$M(x, y, z) = G(y, z) + x[y^2\kappa_z + \Gamma_a(y, z)], \tag{3.1a}$$

where the unknown functions $G(y, z)$ and $\Gamma_a(y, z)$ satisfy

$$\Gamma_a(y, z)G_{zzz} + y(y^2\kappa_{zz} + \Gamma_{a,z})G_{yzz} - y(y^2\kappa_{zzz} + \Gamma_{a,zz})G_{yz} = y^2\kappa G_{zzzz}, \tag{3.1b}$$

$$\begin{aligned} y^2\kappa_{zzzz}\Gamma_a + \Gamma_a\Gamma_{a,zzz} - y^4\kappa\kappa_{zzzzz} - y^2\kappa\Gamma_{a,zzzz} + y[y^2\kappa_{zz}\Gamma_{a,yzz} + 2y\kappa_{zzz}\Gamma_{a,z} \\ + \Gamma_{a,z}\Gamma_{a,yzz} - 2y\kappa_{zz}\Gamma_{a,zz} - y^2\kappa_{zzz}\Gamma_{a,yz} - \Gamma_{a,yz}\Gamma_{a,zz}] = 0. \end{aligned} \tag{3.1c}$$

Next, recall that SH chose the diffusivity, κ, to be uniform. In this case (3.1) simplifies to

$$M(x, y, z) = G(y, z) + x\Gamma_a(y, z), \tag{3.2a}$$

$$[\Gamma_a G_{zzz} + y\Gamma_{a,z}G_{yzz} - y\Gamma_{a,zz}G_{yz}] = \kappa y^2 G_{zzzz}, \tag{3.2b}$$

$$\Gamma_a\Gamma_{a,zzz} - \kappa y^2\Gamma_{a,zzzz} + y[\Gamma_{a,z}\Gamma_{a,yzz} - \Gamma_{a,yz}\Gamma_{a,zz}] = 0. \tag{3.2c}$$

(3.2a) and (3.2b) should be compared with Eqs. (8.1) and (8.5), respectively, in SH. The main result of SH can be recovered by making the special choice,

$$\Gamma_a(y, z) = y^2 w_E\left(\frac{z^2 - z_0 z}{1 - z_0}\right), \tag{3.3}$$

where z_0 is the depth at which w vanishes. However, this solution has only one

2. For the purposes of this paper, the reader may consider *symmetry reductions* to be a special type similarity solution. More details are given in Paper I, and details of the method used by SH is given in Sections 3 and 4 of their work.

arbitrary function and therefore cannot be the general solution of (3.2c), since the general solution of an nth order PDE contains n arbitrary functions. Therefore the solution of SH corresponds to a special solution of (3.2c) and more general solutions do exist, which are recoverable using the method of Clarkson and Kruskal.

Following SH, we choose a simple solution of (3.2b), which yields the general character of the temperature profile. To obtain this, set $G_y = 0$ and then the solution is given by

$$G_{zzz} = \theta_z = C_1 \exp\left\{\left(\frac{1}{3}z^3 - \frac{1}{2}z_0 z^2\right)\frac{w_E}{\kappa(1 - z_0)}\right\}, \tag{3.4}$$

where C_1 is a constant of integration. In the limit $\kappa \to 0$ SH find

$$G_z = (z - z_0)\hat{C}_1 \mathrm{H}(z - z_0), \tag{3.5}$$

where $\hat{C}_1$ is related to C_1 and $\mathrm{H}(s)$ is the Heaviside step function. This solution may be generalized by use of the transformation ν_1 (see Table 1 and Section 2 of SH) yielding

$$G_z = (z - z_0)\hat{C}_1 \mathrm{H}(z - z_0) + (2z - z_0)\gamma(y), \tag{3.6}$$

and consequently using (2.2ii) and (3.6) one obtains

$$\theta(x, y, z) = -\frac{2y^2 w_E}{(1 - z_0)}(1 - x) + \hat{C}_1 \mathrm{H}(z - z_0), \tag{3.7a}$$

and the corresponding velocity field is

$$u = 2w_E(1 - x)\left(\frac{2z - z_0}{1 - z_0}\right), \quad v = y w_E\left(\frac{2z - z_0}{1 - z_0}\right), \quad w = w_E\left(\frac{z^2 - z_0 z}{1 - z_0}\right). \tag{3.7b}$$

The vertical velocity changes sign at the depth $z = z_0$. The temperature and velocity fields are illustrated in Figure 1 (reproduced from Fig. 2, SH).

The temperature profile shows a front at $z = z_0$ with vertically uniform values above and below. The front separates downwelling warm water in the subtropical gyre and the underlying upwelling of cold, deep water. This frontal solution is controlled by a local convergence of characteristics, which is discussed further in Section 3.b.

From scale analysis of the temperature field, (3.7), we find:

$$\theta_x = \frac{2w_E y^2}{1 - z_0} \sim O(1), \quad \theta_y = -\frac{4w_E y}{1 - z_0}(1 - x) \sim O(1), \quad \lim_{\kappa \to 0} \theta_z = \begin{cases} \infty, & z = z_0; \\ 0, & \text{otherwise.} \end{cases} \tag{3.8}$$

Hence the thermodynamic equation effectively separates into two independent balances: a purely vertical balance between advection and diffusion at $z = z_0$,

$$w\theta_z = \kappa\theta_{zz}, \tag{3.9}$$

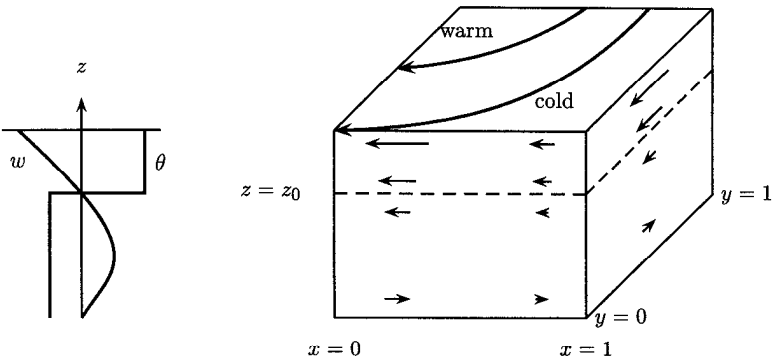

Figure 1. Schematic of the frontal solution corresponding to (3.7), reproduced from Salmon and Hollerbach (1991). A front (dashed line) separates regions of vertically uniform temperature. The vertical velocity (profile at left) is negative throughout the upper layer, positive throughout the lower layer, and zero at the bottom. The horizontal velocities change sign midway through the lower layer.

and elsewhere a horizontal, adiabatic balance,

$$u\theta_x + v\theta_y = 0. \tag{3.10}$$

Thus streamlines are coincident with isotherms in the horizontal plane.

The frontal structure leads to warmer fluid to the west and cooler fluid to the east in the upper layer, so as to provide the anticyclonic circulation in the subtropical gyre. The surface temperature field reflects this underlying frontal variation, as θ_z is zero away from the front. Consequently the surface temperature field appears unrealistic and does not show a polewards decrease (Fig. 1). The implied surface heat flux, $\mathscr{H} = \rho C_p \kappa \theta_z$, is exactly zero, since θ_z is zero.

b. Sensitivity to the vertical velocity profile

SH shows an interior front appearing at the mid-depth at which w vanishes and $\partial w/\partial z < 0$. In this section we examine the control of the front by considering different choices of $\partial w/\partial z$ using piece-wise linear vertical velocity profiles.

We consider the ansatz

$$M(x, y, z) = G(y, z) + xy^2\gamma(z), \tag{3.11a}$$

where

$$\gamma(z) = \begin{cases} \dfrac{w_E(z - z_0)}{1 - z_0} - \epsilon, & z_0 \le z \le 1 \\ \dfrac{w_{\text{bot}}(z_0 - z)}{z_0} - \epsilon, & 0 \le z \le z_0, \end{cases} \tag{3.11b}$$

$0 \le \epsilon \ll |w_E|$ and w_{bot} is the vertical velocity at the bottom of the solution domain. In the limit of constant diffusivity, $w(z) = \gamma(z)$ (see (2.2ii)). Figure 2 illustrates the

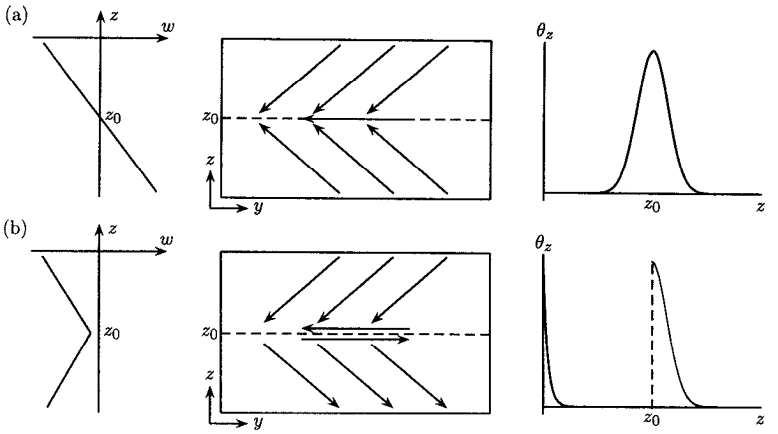

Figure 2. Schematic of the frontal solutions for different velocity boundary conditions: (a) w changes sign at z_0 and (b) the magnitude of w is a minimum at z_0. The vertical velocity profile, characteristics in the yz-plane and the θ_z profile are shown in the left-hand, middle and right-hand columns respectively. A front or boundary layer is formed whenever the vertical velocity profile leads to a local convergence of characteristics. In each case $|w_E| = |w_{\text{bot}}| = 1$ and $z_0 = 0.5$; In case (a) C_1 and C_2 are chosen such that θ_z is continuous at z_0.

vertical velocity profile in the cases $w_E = -1, w_{\text{bot}} = 1$ with $\epsilon = 0$, and $w_E = w_{\text{bot}} = -1$, with $\epsilon > 0$; $z_0 = 0.5$ for each.

The bottom boundary conditions is now altered to $w = w_{\text{bot}}$ at $z = 0$, although the upper boundary condition remains as $w = w_E$ at $z = 1$, and we ensure that the eastern condition at $x = 1$ is satisfied by using the method employed in Section 3.c. We have $\Gamma_a(y, z) = y^2\gamma(z)$ and again (3.2c) is identically satisfied. Hence to ensure that (3.11) is a solution of the thermocline equation, (2.3), it remains to satisfy (3.2b). As before, we set $G_y = 0$; the general character of the temperature profile is unaffected (see Appendix A). (3.2b) becomes

$$\gamma(z)G_{zzz} = \kappa G_{zzzz}, \tag{3.12}$$

which represents a vertical balance between advection and diffusion of heat. Hence integrating we obtain,

$$\theta_z = G_{zzz} = \begin{cases} C_1 \exp\left\{\frac{1}{\kappa}\left[\frac{w_E}{(1-z_0)}\left(\frac{1}{2}z^2 - z_0 z\right) - \epsilon z\right]\right\}, & z_0 \le z \le 1, \\ C_2 \exp\left\{\frac{1}{\kappa}\left[\frac{w_{\text{bot}}}{z_0}\left(z_0 z - \frac{1}{2}z^2\right) - \epsilon z\right]\right\}, & 0 \le z \le z_0, \end{cases} \tag{3.13}$$

where C_1 and C_2 are constants of integration.

SH argues that the position of the internal front is controlled by both the position at which w vanishes and the condition $\partial w/\partial z < 0$; this second condition implies, from linear vorticity balance, that the geostrophic flow is equatorwards in the interior.

This control of the front is illustrated by considering these two different profiles in vertical velocity.

Firstly, when there is surface Ekman pumping with upwelling from the bottom Ekman layer (Fig. 2a), there is equatorward flow throughout the interior. The characteristics map the mean streamlines in the *yz*-plane and reveal how information propagates into the domain from the boundaries. In this case, the characteristics emanate from the upper and lower boundaries and converge at the mid-depth $z = z_0$. This leads to a front in any passive tracer at $z = z_0$ unless either the boundary conditions for the tracer are uniform, or diffusion is sufficiently large to smear out the feature. The profile in θ_z shows the front located at $z = z_0$ with θ elsewhere being relatively uniform in the vertical (Fig. 2a).

Secondly, consider the less realistic case of surface Ekman pumping with downwelling in the bottom Ekman layer (Fig. 2b). Again there is equatorward flow between the surface and mid-depth $z = z_0$, but now polewards flow from there to the seafloor. Consequently, characteristics emanate from the upper boundary and converge just above $z = z_0$, which leads to a front in θ lying just above $z = z_0$. However, below $z = z_0$, the characteristics diverge and spread out to the lower boundary. As SH argue, this leads to θ having a boundary layer at the seafloor. The temperature profile now is more complex and shows an asymmetrical front lying just above z_0 together with a lower boundary layer at the seafloor (Fig. 2b). These examples illustrate how the front is controlled by the local convergence of characteristics and it is not necessary to have convergence from both upper and lower boundaries (although this later case is more plausible).

SH show the control of a front in the more realistic case of the wind-stress curl varying with latitude with Ekman pumping occurring in a subtropical gyre and Ekman suction in a subpolar gyre. The characteristics for this case are reproduced in Figure 3, again with them representing the streamlines of the mean flow in a meridional section. There is a convergence of characteristics at the mid-depth z_0 in

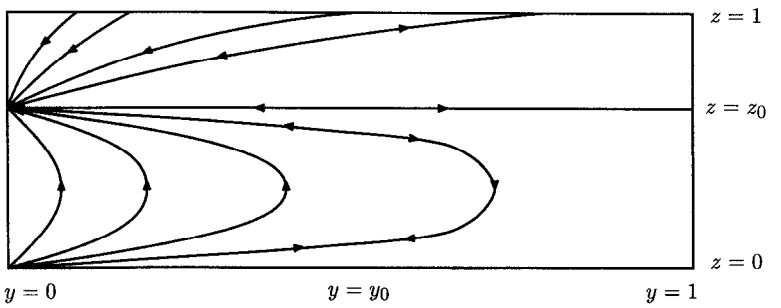

Figure 3. A north-south section showing the characteristic lines corresponding to a subtropical and subpolar gyre solution reproduced from Salmon and Hollerbach, 1991. These characteristic lines are streamlines for the velocity field projected onto the *yz*-plane; the arrows indicate the direction of flow. There is a local convergence of characteristics at $z = z_0$ in the subtropical gyre, whereas a divergence occurs at $z = z_0$ in the subpolar gyre.

the subtropical gyre ($0 \leq y < y_0$), whereas there is a divergence at that depth in the subpolar gyre ($y_0 < y < 1$). Consequently, the SH solutions show an internal front occurring over the subtropical gyre and not over the subpolar gyre, which is broadly in accord with observations showing a stronger main thermocline over a subtropical gyre. Their solution shows how the frontal character results from the interaction of the anticyclonic wind-driven gyre with the underlying thermohaline circulation.

c. Sensitivity to the diffusivity profile

The sensitivity of the frontal solution to diffusion is now examined by allowing κ to vary with depth. The diffusivity is chosen to be

$$\kappa(z) = \lambda z^3 \tag{3.14}$$

where λ is positive and remains to be set; this form automatically leads to zero heat flux on the seafloor (1.6). This choice extends the case considered by SH and, more realistically, allows an increase in diffusivity toward the sea surface, while it is still analytically tractable. The case is used to analytically prove the existence of a front; see Appendix B.

We use the same reduction as in Section 3.a, i.e., (3.1). Choosing $\Gamma_a(y, z)$ to be quadratic in z, i.e.,

$$\Gamma_a(y, z) = y^2(\gamma_{2a}z^2 + \gamma_{1a}z + \gamma_{0a}), \tag{3.15}$$

as before (cf. (3.3)), ensures (3.2c) is identically satisfied, and generalizing (3.1a) by using ν_1 again (see (3.5) and (3.6)), we obtain

$$M(x, y, z) = G(y, z) + y^2(x + x_0(y))[(3\lambda + \gamma_{a2})z^2 + \gamma_{a1}z + \gamma_{a0}], \tag{3.16}$$

where $x_0(y)$ is the arbitrary function introduced by ν_1.

We now apply our three boundary conditions: $w \to 0$ as $z \to 0$, hence $\gamma_{a0} = 0$; $w \to w_E$, as $z \to 1$, hence $\gamma_{1a} = w_E - 3\lambda - \gamma_{a2}$. Computing u from (2.2i) and (3.16), substituting into (2.6) and performing the z integration, our eastern boundary condition becomes

$$\int_0^1 (yx_{0,y} + 2x_0(y) + 2)dy = 0. \tag{3.17}$$

We may choose *any* function, $x_0(y)$, which satisfies (3.17).

Again we set $G_y = 0$. The velocity and temperature fields are now straightforward to find from (2.2) and (3.16), and are as follows:

$$u = (yx_{0,y} + 2x_0(y) + 2x)(\gamma_{2a} + 3\lambda - w_E - 2z(3\lambda + \gamma_{2a})), \tag{3.18a}$$

$$v = [2(3\lambda + \gamma_{2a})z + (w_E - 3\lambda - \gamma_{2a})]y, \tag{3.18b}$$

$$w = (3\lambda + \gamma_{2a})z^2 + (w_E - 3\lambda - \gamma_{2a})z, \tag{3.18c}$$

$$\theta = \theta_0 + \int G_{zzz}dz + 2(3\lambda + \gamma_{2a})y^2(x + x_0(y)). \tag{3.18d}$$

We now address the problem of determining the temperature profile, i.e., of computing G_{zzz} (cf. 3.18d).

Firstly, to help physical interpretation of the results it is convenient to introduce z_0, the depth at which the vertical velocity goes to zero. From (3.18c) we find

$$z_0 = 1 - \frac{w_E}{3\lambda + \gamma_{2a}}. \tag{3.19}$$

With $G_y = 0$ (3.1b) simplifies to

$$\left(\frac{(z - z_0)w_E}{(1 - z_0)z^2} - \frac{3\lambda}{z}\right)G_{zzz} = \lambda G_{zzzz}, \tag{3.20}$$

which has solution,

$$G_{zzz}(z) = C_1 \exp\left\{\frac{1}{\lambda}\left[\left(\frac{w_E}{1 - z_0}\right)\ln z + \frac{z_0 w_E}{(1 - z_0)z}\right]\right\}, \tag{3.21}$$

where C_1 is a constant of integration. The resulting θ and θ_z profiles are shown in Figure 4; the plots are nondimensionalized with $C_1 = 1$ — the dimensional value of C_1 depends on the surface and bottom temperatures, i.e., θ_{bot} and θ_{surf}, and is given by

$$C_1(\lambda) = \frac{\theta_{bot} - \theta_{surf}}{\int_0^1 \exp\left\{\frac{1}{\lambda}\left[\left(\frac{w_E}{1 - z_0}\right)\ln z + \frac{z_0 w_E}{(1 - z_0)z}\right]\right\}dz}. \tag{3.22}$$

This integral appears intractable except in the case where γ_{2a}/λ is an integer.

The temperature and surface velocity fields corresponding to the choice

$$yx_{0,y} + 2x_0(y) = -3\cos(\pi[y - 0.11]), \tag{3.23}$$

are now discussed.

Thermocline solutions are shown in Figure 4, for this variable diffusivity case, $\kappa = \lambda z^3$, with three different choices in λ. As expected, the θ profile is relatively smooth and continuous for high λ, whereas the frontal character reappears for small λ (compare Fig. 4a and c). This is more clearly shown in the accompanying θ_z profile and reveals how the maximum gradient is always centered around $z = z_0$.

These thermocline solutions are compared with those for constant κ in which the constant value is set to $\kappa = \lambda z_0^3$, which is the same value at $z = z_0$ as for the previous variable cases. The similarity between the θ_z profiles in these variable and constant cases in Figure 4 suggests that the frontal solutions are controlled by the local value of κ at $z = z_0$, rather than by the surface value or depth-mean value. Consequently the frontal character of these solutions appears robust to these changes in diabatic forcing away from the depth $z = z_0$.

However, the surface θ field is sensitive to these choices in κ, as revealed in Figure 5.

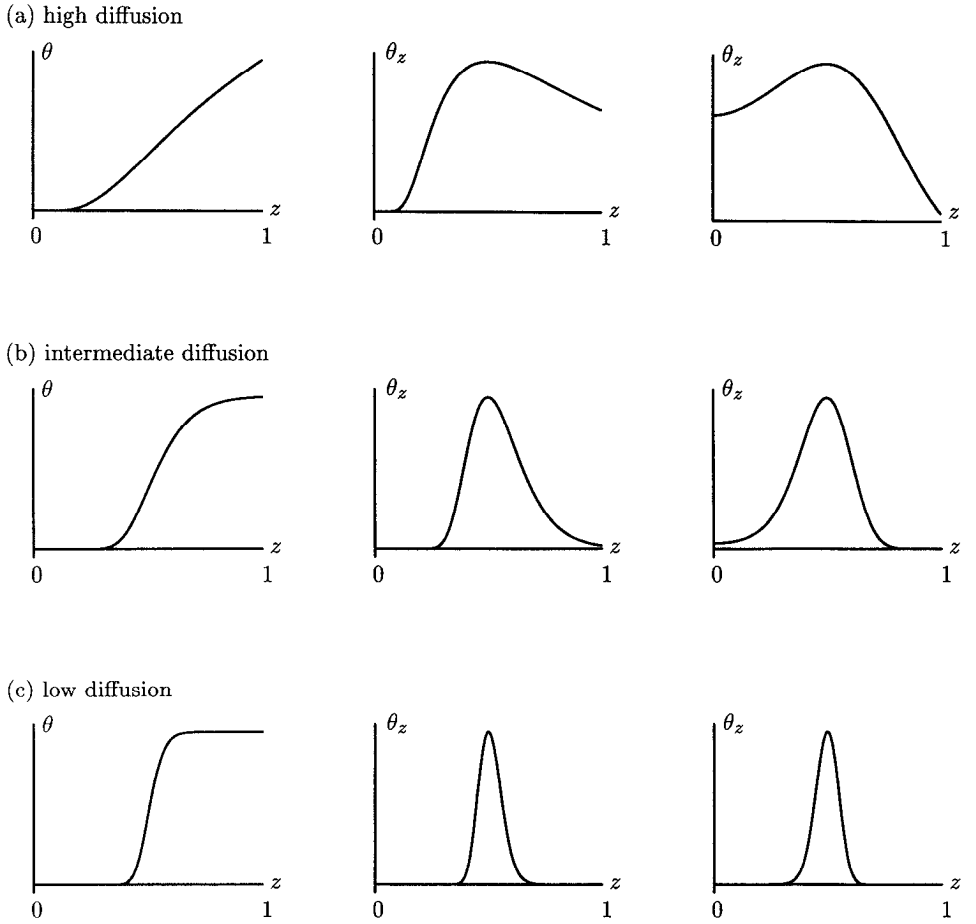

Figure 4. The θ and θ_z profiles for a depth-varying diffusivity, $\kappa(z) = \lambda z^3$, are shown in the left-hand and middle columns, respectively. The magnitude of the diffusivity decreases from (a) to (c), with the following values: (a) $\lambda = 1.0$, (b) $\lambda = 0.1$ and (c) $\lambda = 0.02$. The interior front is clearly seen by the mid-depth maximum in θ_z, occurring at $z = z_0$. The corresponding θ_z profile with the same uniform value of κ as in the previous case at $z = z_0$ is shown in the right-hand column. In each case we have set $w_E = -1, z_0 = 0.5$ and, for convenience, $C_1 = 1$; although in reality C_1 depends on λ.

In the low diffusivity case, in Figure 5a, the isotherms and streamlines are nearly coincident. In the high diffusivity case, in Figure 5b, there is more cross-isothermal flow and the θ field shows a more plausible polewards decrease. Consequently, while the variable κ does not appear to alter the frontal character when $\kappa(z_0)$ becomes small, the near surface values of κ do alter the surface temperature fields. The implied surface heat flux into the ocean, $\mathscr{H} = \rho C_p \kappa \theta_z$, is effectively zero in the small κ case due to the form of θ_z (see Fig. 4(c) and the SH case). The surface heat flux increases in

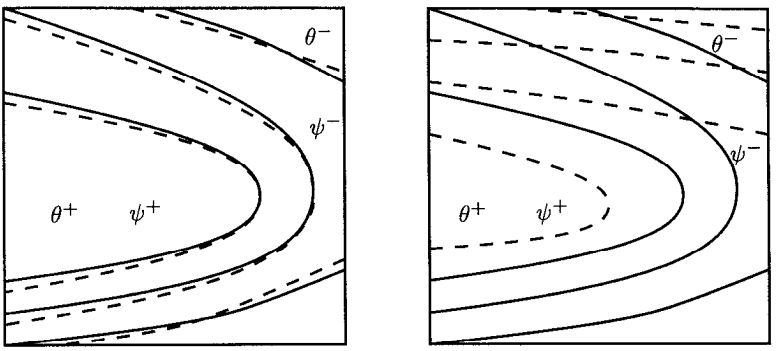

Figure 5. Surface streamlines and isotherms (continuous and dashed respectively) for variable diffusivity, $\kappa(z) = \lambda z^3$, with (a) a low diffusive value of $\lambda = 0.1$ and (b) a high diffusive value of $\lambda = 1.0$. The cross-isothermal flow increases in the more diffusive case. Physical choices of $x_0(y)$ (from (3.23)) and constant parameters are made with $w_E + \gamma_{2a} + 3\lambda < 0$ and $3\lambda + \gamma_{2a} < 0$.

magnitude in the larger κ cases and remains spatially uniform due to θ_z being independent of x and y in these solutions (see 3.25c).

One can infer the physical processes controlling the formation of the thermocline by determining the relative sizes of the terms in the thermodynamic equation (2.1c):

$$u\theta_x + v\theta_y + w\theta_z = (\kappa\theta_z)_z. \tag{3.24}$$

From (3.18d) we find,

$$\theta_x = 2(3\lambda + \gamma_{2a})y^2, \tag{3.25a}$$

$$\theta_y = 2(3\lambda + \gamma_{2a})y(2x - 3\cos(\pi[y - 0.11])), \tag{3.25b}$$

$$\theta_z = G_{zzz} = C_1 z^{\gamma_{2a}/\lambda} \exp\left(\frac{3\lambda + \gamma_{2a} - w_E}{\lambda z}\right). \tag{3.25c}$$

Since we have nondimensionalized the Thermocline System, then terms on the right-hand side of (3.18a), (3.18b), (3.18c), (3.25a) and (3.25b) are $O(1)$, hence so are $u\theta_x$ and $v\theta_y$, the first two terms in (3.24) — one can exclude 'pathological' cases of the $x_0(y)$ for realistic solutions. Determining the size of $w\theta_z$ is more difficult, since the size of θ_z depends strongly on the size of λ. The analysis in Appendix B shows that if $\lambda = O(1)$ then $\theta_z = O(1)$, whereas as $\lambda \to 0$ then $\theta_z \to O(1)$ at $z = z_0$, i.e., a front is formed.

From these similarity solutions we conclude that there are still frontal solutions even with a variable diffusivity profile and that the vertical advection and diffusion of heat are always comparable in magnitude, or larger than, the horizontal advection terms.

The potential vorticity balance is given by

$$uq_x + vq_y + wq_z = (\kappa q)_{zz}, \tag{3.26}$$

where $q = y\theta_z$. As θ_z is spatially uniform in the horizontal (cf. 3.25c), then q_x is zero and (3.26) simplifies to

$$vq_y + wq_z = (\kappa q)_{zz}. \tag{3.27}$$

This two-dimensional balance is the same as that obtained by SH in the variable Ekman pumping case, which is used to plot the characteristics along a meridional section in Figure 3.3.

In the next section we examine the alternative limit in a ventilated model where the vertical advection balances horizontal advection, rather than vertical diffusion in the interior.

4. Ventilated solutions

a. Methodology

Ventilated models emphasize the role of the surface boundary in setting the structure of the underlying thermocline. LPS impose the surface temperature field and solve for the underlying stratification using a layered model. In contrast, Salmon (1990) casts doubt on the LPS solutions and argues that the surface temperature should be solved for, rather than imposed. In this study we wish to obtain ventilated solutions using the similarity approach. To make analytical progress we choose the limit of moving fluid having uniform potential vorticity, $q = y\theta_z$ (cf. Marshall and Nurser, 1991), which replaces the previous choice of $G_y = 0$ in the frontal solutions in Section 3. The diabatic forcing is chosen to be confined to a surface layer overlying an adiabatic interior. While these ventilated solutions automatically avoid the frontal limit through the choice of q, they do illustrate how a continuous thermocline may be formed with appropriate diabatic forcing and boundary conditions.

We consider a solution which we obtain from Reduction 3.2.1, Paper I. This reduction is given by

$$M(x, y, z) = \lambda_1^{-1} y^{\gamma_0} G(\xi, z) + \left(\frac{\gamma_2}{2\lambda_1} z^2 - \frac{\lambda_2}{\lambda_1} z\right) \int y^{\gamma_0 - 1}\, dy + \alpha_0(y) + Az^2, \tag{4.1a}$$

$$\xi = \lambda_1 x y^{2-\gamma_0} + \phi(y), \tag{4.1b}$$

where $\phi(y)$, γ_0, γ_2 and λ_1 remain arbitrary, and $G(\xi, z)$ satisfies

$$G_\xi G_{zzz} - \kappa(z) G_{zzzz} - \kappa_z G_{zzz} + \gamma_0 (G_{\xi z} G_{zz} - G_z G_{\xi zz}) + \left(\frac{\lambda_2 - z}{\lambda_1}\right) G_{\xi zz} + \gamma_2 G_{\xi z} = 0. \tag{4.1c}$$

Note that we have in fact generalized Reduction 3.2.1 slightly by the transformation $M \to M + Az^2$, i.e., ν_7, (Table 1, SH) where A is an arbitrary constant (cf. the note on ν_1, in Section 3.a, above). Further, we set $\alpha_0 = 0$ since it plays no physical role.

Assuming potential vorticity, $q = yM_{zzz}$ (cf. (2.4)), is uniform and substituting (4.1a) into (2.4) leads to the requirements,

$$\gamma_0 = -1, \qquad G(z, \xi) = z^3G_3(\xi) + z^2G_2(\xi) + zG_1(\xi) + G_0(\xi). \tag{4.2}$$

Given that $G(\xi, z)$ is cubic in z (cf. (4.2)) then from (4.1c) we see that $\kappa(z)$ is at most quartic, i.e.,

$$\kappa(z) = k_4z^4 + k_3z^3 + k_2z^2 + k_1z, \tag{4.3}$$

where $k_1, \ldots, k_4$ are to be specified. In the real ocean diffusion varies by several orders of magnitude between the surface boundary layer and interior, and (4.3) does not admit such variation. Hence we split out solution domain into two regimes (Fig. 3): an upper *surface boundary layer,* in which diffusion is given by (4.3), and a deeper *ocean interior* in which diffusion is assumed to be negligible and we set $\kappa = 0$, i.e.,

$$M(x, y, z) = \begin{cases} M^S(x, y, z), & z_i \le z \le 1, \quad \kappa \ne 0; \\ M^I(x, y, z), & 0 \le z \le z_i, \quad \kappa = 0. \end{cases} \tag{4.4}$$

Then substituting (4.2) and (4.3) into (4.1c), and equating coefficients of like powers of z yields the system,

$$G_{3,\xi} - 4k_4 = 0, \tag{4.5a}$$

$$24k_4G_2 = 18k_3G_3 - 12\gamma_2k_4 + 24k_4\lambda_1^{-1}, \tag{4.5b}$$

$$6G_1G_{3,\xi} = 12k_2G_3 - 6\lambda_1^{-1}\lambda_2G_{3,\xi} + 2(\lambda_1^{-1} - \gamma_2)G_{2,\xi}, \tag{4.5c}$$

$$6G_3G_{0,\xi} = (2G_2 - \gamma_2)G_{1,\xi} - 2(G_1 + \lambda_1^{-1}\lambda_2)G_{2,\xi} + 6k_1G_3. \tag{4.5d}$$

Superscripts are omitted here, since the system applies to both the upper and lower layers. For generic values of the parameters, $k_1, \ldots, k_4$, γ_0, λ_1 and λ_2, we have an exactly-determined system of equations for $G_0(\xi) \ldots G_3(\xi)$, so the solution has no arbitrary functions with which to match boundary conditions. However, we choose nongeneric values, based on our physical prejudices (Fig. 6).

Ocean interior. In this layer $\kappa = 0$ (so $k_4^I = k_3^I = k_2^I = k_1^I = 0$) so G_3^I is necessarily constant, (4.5b) vanishes, and (4.5c) and (4.5d) become

$$2[(\lambda_1^I)^{-1} - \lambda_2^I]G_{2,\xi^I}^I = 0, \tag{4.6a}$$

$$[G_1^I + (\lambda_1^I)^{-1}\lambda_2^I]G_{2,\xi^I}^I + (\lambda_2^I - 2G_2^I)G_{1,\xi^I}^I = 0, \tag{4.6b}$$

respectively.

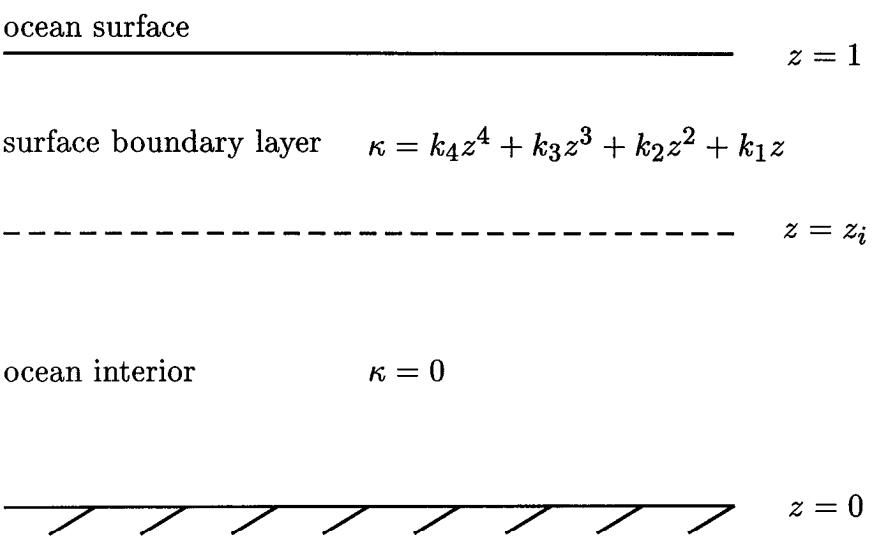

Figure 6. Schematic showing the assumed diffusion profile: in the surface boundary layer, diffusion varies with depth and is significant, while in the ocean interior it is zero everywhere. A solution is obtained in each layer and we require that w and θ match at the interface.

Surface Boundary Layer. If we choose

$$k_4^S = k_3^S = 0, \tag{4.7}$$

then G_3^S is necessarily constant, (4.5b) vanishes and integrating (4.5c) we obtain

$$G_2^S(\xi^S) = g_{20}^S - \frac{6g_3 k_2 \xi^S}{(\lambda_1^S)^{-1} - \gamma_2} \equiv g_{20}^S + \hat{k}_2 \xi^S, \qquad \frac{1}{\lambda_1^S} - \gamma_2^S \neq 0, \tag{4.8}$$

where we have introduced $\hat{k}_2$ which is defined in the obvious way. It remains to obtain $G_0^S(\xi^S)$ from (4.5d) which becomes

$$G_0^S = g_{00}^S + \frac{1}{6g_3^S} \int \{6k_1^S g_3^S + [2G_2^S(\xi^S) - \gamma_2] G_{1,\xi^S}^S - 2[G_1^S(\xi^S) + (\lambda_1^S)^{-1}\lambda_2^S] G_{2,\xi^S}^S\} \, d\xi, \tag{4.9}$$

where g_{00} is a constant of integration and $G_1^S(\xi^S)$ is determined by surface boundary conditions.

Boundaries and the interface. Using (2.2ii) and (4.1a), and evaluating at $z = 1$ we find the surface temperature field to be

$$\theta_{\text{surf}} = M_{zz|_{z=1}} = \frac{1}{\lambda_1^S y} [6g_3^S + 2G_2^S(\xi) - \gamma_2^S] + 2A^S, \tag{4.10}$$

so $G_2^S(\xi)$ (which is given by (4.8)) is constrained by θ_{surf}—the functional form of $\xi(x, y)$ and therefore the choice of $\phi(y)$ (cf. 4.1b) is important here—and our remaining arbitrary function in the surface boundary layer, $G_2^S(\xi^S)$, is determined by our other surface condition, the Ekman pumping, where

$$w_E(x, y) = y^{-2}M_{x|z=1} = G_{2,\xi}^S + G_{1,\xi}^S + G_{0,\xi}^S \tag{4.11}$$

(using (2.2i) and (4.1a)).

At depth, i.e., as $z \to 0$, we assume $w \to 0$, and since $w \to G_{0,\xi}^I$, then G_0^I is necessarily constant.

At the interface between the two regimes, i.e., at $z = z_i$, we require that w and θ be continuous, i.e.,

$$M_x^S(x, y, z_i) \equiv M_x^I(x, y, z_i), \tag{4.12}$$

$$M_{zz}^S(x, y, z_i) \equiv M_{zz}^I(x, y, z_i). \tag{4.13}$$

The simplest way to satisfy these interface conditions is to choose identical similarity variables in each regime; hence

$$\lambda_1^S = \lambda_1^I, \qquad \phi^S(y) \equiv \phi^I(y) \tag{4.14}$$

and we drop the superscripts on these variables. (4.12), (4.13) together with (4.6), then becomes a coupled system of ODEs for $G_1^I(\xi)$ and $G_2^I(\xi)$. It is an over-determined system. However, if we choose

$$1 - \lambda_1\gamma_2^I = 0, \tag{4.15}$$

(4.6a) vanishes; the system is still over-determined, but less strongly. Even though the system is over-determined, there is a family of solutions that satisfy the applied boundary conditions.

Finally we consider the eastern boundary condition (cf. (2.6)). This becomes

$$\int_{z=0}^{z=z_i}\int_{y=0}^{y=1} u^I(x = 1, y, z)\, dydz + \int_{z=z_i}^{z=1}\int_{y=0}^{y=1} u^S(x = 1, y, z)\, dydz = 0 \tag{4.16}$$

and determines one of the parameters in our solution in terms of the others.

b. Example of a subtropical gyre

These similarity solutions are computed for an idealized subtropical gyre with uniform Ekman pumping, as well as assuming a simple form for $\phi(y)$:

$$w_E(x, y) = w_{E0} < 0, \tag{4.17a}$$

$$\phi(y) = \lambda_1\phi_0 y^4, \tag{4.17b}$$

where ϕ_0 is a constant and is to be determined. The derivation of the resulting velocity and temperature fields is straightforward and shown in Appendix C. The

Table 1. The temperature and velocity fields for the ventilated solutions with uniform Ekman pumping over the subtropical gyre (4.17). Variables in the surface boundary layer and interior are identified by a superscript S or I respectively. There is no diffusion in the interior, so the streamlines and isotherms coincide; hence, we omit the horizontal velocity fields in this case.

$$\theta^S = 2\hat{k}_2(xy^2 + \phi_0 y^3) + 2A^S + \frac{1}{\lambda_1 y}(6zg_3^S + 2g_{20}^S - \gamma_2^S); \qquad 6g_3^S + 2g_{20}^S - \gamma_2^S = 0,$$

$$\theta^I = \frac{1}{\lambda_1 y}(6g_3^I z + C_1) + 2C_2(xy^2 + \phi_0 y^3) + 2A^I$$

$$u^S = -(2x + 3\phi_0 y)\{w_{E0} + \hat{k}_2(2z - 1 - 2g_{00}^S)\}$$

$$+ \frac{1}{\lambda_1 y^3}\left\{3g_3^S z^2 + (2g_{20}^S - \gamma_2^S)z + h_0 - g_{20}^S + \lambda_2^S + \frac{\hat{k}_1}{2\hat{k}_2}\right\}$$

$$v^S = y\{w_{E0} + \hat{k}_2(2z - 1 - 2g_{00}^S)\}$$

$$w^S = w_{E0}z + (2g_{00}^S - z)(1 - z)\hat{k}_2$$

$$w^I = C_2(z + 2g_{10}^I)z$$

$$C_1 = -\gamma_2^I + \frac{2}{z_i(z_i + 2g_{10}^I)}\left\{g_{20}z_i^2 + (w_{E0} - \hat{k}_2 - 2g_{00}^S\hat{k}_2)z_i + g_0^I - \frac{\hat{k}_1}{2\hat{k}_2}\right\}$$

$$C_2 = \frac{1}{z_i(z_i + 2g_{10}^I)}\{z_i^2\hat{k}_2 + (w_{E0} - \hat{k}_2 - 2g_{00}^S\hat{k}_2)z_i + 2g_{00}^S\hat{k}_2\}$$

relations for the velocity and temperature fields are shown in Table 1. These solutions satisfy our imposed surface and bottom conditions, as well as the requirement that w is continuous across the interface at $z = z_i$. It remains to ensure that temperature is continuous across this interface and that our condition of no net flow through the eastern boundary is satisfied. The former condition requires

$$(3z_i g_3^S + 2g_{20}^I - 3z_i g_3^I) = 2(z_i^2 g_{20}^S + z_i(w_E - \hat{k}_2 - 2g_{00}^S\hat{k}_2) + 2g_{00}^S g_{20}^S, \qquad (4.18)$$

and the latter, expressed mathematically by (4.16), simply places another algebraic constraint on the various parameters in the system and affects only the details of the flow.

Note that in order to avoid a singularity at the surface as $y \to 0$ we have chosen to impose the algebraic constraint

$$6g_3^S + 2g_{20}^S - \gamma_2^S = 0. \qquad (4.19)$$

All temperature contours, $\theta_0 = \theta(x_0, y, z)$ now tend to a point immediately below the surface.

Finally, it is simple to ensure the continuity of the pressure field over the interface by choosing the free parameters in the model appropriately, for example A^S and A^I.

c. Temperature field and thermodynamic balances

Surface and interior temperature field. The surface temperature field is obtained by setting $z = 1$ in the expression for θ^S in Table 1,

$$\theta_{\text{surf}} = 2\hat{k}_2(xy^2 + \phi_0 y^3) + 2A^S, \tag{4.20}$$

and imposing the conditions

$$\hat{k}_2 < 0, \qquad \phi_0 > 0, \tag{4.21}$$

means that surface temperature decreases both northward and eastward. Further, the potential vorticity is piecewise constant within each layer and by definition is positive

$$q^S = 6\frac{g_3^S}{\lambda_1} > 0, \qquad q^I = 6\frac{g_3^I}{\lambda_1} > 0. \tag{4.22}$$

The components of $\nabla\theta$ in the seasonal boundary layer and interior are given by

$$\theta_x^S = 2\hat{k}_2 y^2, \quad \theta_y^S = 2\hat{k}_2(2xy + 3\phi_0 y^2) - \frac{1}{\lambda_1 y^2}(6zg_3^S + 2g_{20}^S), \quad \theta_z^S = \frac{6g_3^S}{\lambda_1 y}, \tag{4.23a}$$

$$\theta_x^I = 2C_2 y^2, \quad \theta_y^I = 2C_2(2xy + 3\phi_0 y^2) - \frac{1}{\lambda_1 y^2}(6g_3^I z + C_1), \quad \theta_z^I = \frac{6g_3^I}{\lambda_1 y}, \tag{4.23b}$$

where C_1 and C_2 are constants defined in Table 1. Scale analysis of the thermodynamic equation shows that all the terms from (4.23) are relevant in the surface boundary layer,

$$u\theta_x + v\theta_y + w\theta_z = (\kappa\theta_z)_z, \tag{4.24}$$

whereas there is a balance between the horizontal and vertical advective terms in the adiabatic interior,

$$u\theta_x + v\theta_y + w\theta_z = 0. \tag{4.25}$$

These thermodynamic balances are broadly in accord with those used in ventilation models (although the θ_z term is zero in a mixed layer). They are in contrast to those of SH, where vertical advection balances vertical diffusion at the front (3.9), and elsewhere there is a horizontal, adiabatic flow (3.10).

d. Discussion of result

The structure of the thermocline is shown as a meridional section across the subtropical gyre in Figure 7. The thermocline is automatically continuous through

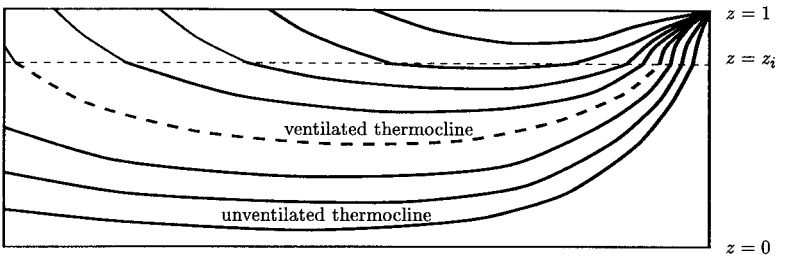

Figure 7. North—South section of the temperature field corresponding to the similarity solutions given in Table 1 for a subtropical gyre with uniform Ekman pumping. There is a diabatically forced surface boundary layer (above thin dashed line at z_i), which overlies an adiabatic interior. Fluid is subducted from the surface boundary layer and forms a ventilated thermocline (above thick dashed line), which overlies moving fluid in an unventilated thermocline.

the choice of uniform potential vorticity. The diabatically forced flow is confined to the surface boundary layer above $z = z_i$ and there is adiabatic flow below in the interior. The potential vorticity is chosen to have a higher value in the interior, than the surface boundary layer, which leads to the change in slope of the isotherms across the interface z_i. Conservation of potential vorticity along streamlines within the adiabatic interior leads to the equatorwards reduction in the spacing between θ surfaces. This meridional structure is similar to that obtained by Welander (1971), although the singularity at the equator is probably an unphysical consequence of assuming uniform Ekman pumping and potential vorticity. The adiabatic thermocline is separated into a ventilated regime, where fluid is subducted from the surface boundary layer into the interior, and an unventilated regime, where fluid is insulated from the diabatic forcing within the subtropical gyre; this separation also occurs in the extension of the LPS model by Huang (1988).

The resulting surface θ distribution appears more realistic in this ventilated limit, than in the previous cases (compare Figure 1 with 8a). There is now a poleward decrease in surface temperature throughout the subtropical gyre with a strong cross-isothermal flow (Fig. 8). The implied surface heat flux into the ocean, $\mathscr{H} = \rho C_p \kappa \theta_z$, is inversely proportional to y and is independent of x (see form of θ_z in (4.23) and Fig. 8b). The heat flux drives both the cross-isothermal geostrophic flow and the vertical downwelling of heat. This supply of heat originates from the atmosphere or the horizontal convergence of the Ekman heat flux, as there is an implied Ekman layer overlying the model domain.

These similarity solutions broadly capture the dynamical balances emphasized in ventilation models, even though the flow and θ distributions are solved for, rather than imposed (albeit with uniform q). Consequently, ventilated solutions appear to be relatively robust to whether a layered or similarity approach is applied.

In practice, it is unrealistic to expect the surface boundary conditions to conveniently supply uniform potential vorticity into the interior of the subtropical gyre,

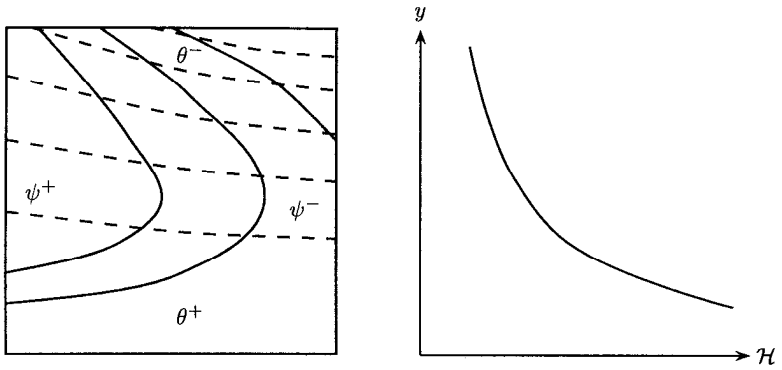

Figure 8. (a) A plan view of the surface steamlines and isotherms (continuous and dashed lines respectively) corresponding to the ventilated solutions given in Table 1. (b) The meridional variation of the implied surface heat flux directed into the ocean. The heat flux increases equatorward and is independent of x (the exact value can be tuned in the solutions).

although, this limit can easily occur for some θ surfaces using mixed-layer boundary conditions from the end of winter (see Williams, 1991). Therefore, we would expect a more realistic model to provide a range in the value of potential vorticity subducted into the interior, which would modify the structure of the ventilated thermocline.

5. Discussion and conclusions

The ubiquitous feature of the main thermocline in the ocean has stimulated an extensive debate with different models invoking advective or diffusive balances in the thermodynamic equation. In particular, Salmon and Hollerbach (SH) suggest that the thermocline is an interior front in the subtropical gyre in the limit of vanishing diffusivity, whereas Luyten *et al.* (LPS) argue that the thermocline is controlled by advection sweeping the surface temperature field into the ocean interior. Reconciling these explanations has been made more difficult through each study employing different model formulations and making different physical assumptions.

In this study, a similarity approach is used to solve for the entire velocity and temperature field in an idealized subtropical gyre away from the lateral boundaries. The diabatic forcing is chosen to be represented simply by a vertical diffusion of heat with the diffusivity varying with depth. Our main results are discussed here in terms of solutions broadly corresponding with the SH and LPS limits together with intermediate cases.

In the SH limit, an interior front appears over the subtropical gyre as the vertical diffusivity becomes vanishingly small. The front occurs at mid-depth where w changes sign and separates an upper regime of downwelling, warm fluid from a lower regime of upwelling, cool fluid. Consequently, the front is due to the interaction of an

anticyclonic gyre and the underlying thermohaline circulation. The resulting surface temperature field appears though unrealistic with isotherms coincident with streamlines and the implied surface heat flux is exactly zero.

The frontal solutions are found to be relatively robust to our changes in the vertical velocity and vertical diffusivity. The front is formed through a local convergence of characteristics occurring where $w \to 0$ and $\partial w/\partial z < 0$ in the limit of small diffusivity, κ. Modifying the vertical diffusivity profile elsewhere is found not to significantly alter the frontal solution. However, a surface increase in κ and corresponding increase in implied surface heat flux leads to more plausible surface fields with streamlines crossing isotherms, rather than being constrained to be coincident. It is unclear though whether these frontal solutions are still sensitive to a different parameterization of diabatic forcing, such as one representing the stirring by geostrophic eddies (Rhines and Young, 1982; Gent *et al.*, 1995).

In the contrasting ventilation limit, the same similarity approach is applied, but the diffusivity is chosen now to be large in a surface layer and zero in the underlying interior; this choice crudely represents how the diabatic forcing is observed to be concentrated at the surface. As in LPS and other ventilation models, the deep waters are crucially assumed to be motionless. The similarity solutions show that a continuous thermocline is formed through the circulation sweeping the surface temperature field into the interior. This ventilated thermocline is not restricted to the diabatically-forced surface layer and does not have a frontal character. There is now a more realistic surface temperature field with a polewards decrease in temperature, than in the SH case. In the underlying interior, there is adiabatic flow with a balance between horizontal and vertical advection of heat. Consequently, this similarity solution has similar dynamical balances to that in LPS, which suggests that the ventilated solutions are robust to different model formulations and in how the surface boundary condition is applied.

In conclusion, the contrasting ventilated and frontal solutions differ because of the physical processes represented, rather than due to their exact formulation. The ventilated thermocline is formed by the advection of the surface temperature field into the interior of the subtropical gyre. The frontal solution is instead formed by the vertical convergence of warm and cold water resulting from the interaction of a subtropical gyre and the thermohaline circulation. Both of these solutions might be relevant to the real ocean, although we have been unable simultaneously to combine them in our study. Recently, Samelson and Vallis (1996a, b) have numerically integrated a modified thermocline equation set with Rayleigh friction and temperature diffusion included. They show the formation of two thermoclines within a subtropical gyre, which might correspond to these ventilated and frontal limits.

Acknowledgments. This work was supported by the NERC UK WOCE Special Topic fund, GST/02/813. We are grateful to an anonymous reviewer for incisive comments and to Geoff Vallis for useful discussions.

APPENDIX A

In this section we substantiate the claim that setting $G_y = 0$ does not change the general character of the velocity or temperature fields (cf. Sections 3.a and 3.b). To do this we assume

$$\Gamma_a(y, z) = f(y)\gamma(z), \tag{A.1i}$$

$$G(y, z) = g(y)\sigma(z), \tag{A.1ii}$$

where $f(y)$, $g(y)$, $\gamma(z)$ and $\sigma(z)$ are to be determined. From (3.2c) it immediately follows that $f(y) = f_0 y^2$, where f_0 is constant and then to avoid obtaining an over-determined system of ODEs for $\gamma(z)$ and $\sigma(z)$, from (3.2b) we find $g(y) = g_0 y^n$, where both g_0 and n are constant. Assuming $\gamma(z)$ is given by (3.11b) $\sigma(z)$ satisfies

$$[(w_E - w_{\text{bot}})z + w_{\text{bot}}]g_0\sigma_{zzz} + g_0 n(w_E - w_{\text{bot}})\sigma_{zz} = \kappa\sigma_{zzzz}, \tag{A.2}$$

which is solvable in terms of parabolic-cylinder (Weber-Hermite) functions (Abramowitz and Stegun, 1972, Section 19), viz.,

$$\sigma(z) = C_1\mathscr{P}_1 \exp\left\{\frac{g_0}{\kappa}[(w_E - w_{\text{bot}})z^2 + w_{\text{bot}}z]\right\} + C_2\mathscr{P}_2, \tag{A.3}$$

where C_1 and C_2 are constants of integration, and $\mathscr{P}_1$ and $\mathscr{P}_2$ are known polynomials in z. In the limit in which $\kappa \to 0$ the exponential part of the first term on the r.h.s. of (A.3) dominates and we have recovered (3.13).

APPENDIX B

In this section we show that the maximum value of θ_z, $z \in (0, 1)$, for the intermediate frontal case (cf. Section 3.c, Eq. 3.25c) is small if diffusion is significant, and becomes unbounded as diffusion becomes vanishingly small. That is to say, mathematically speaking, we show that $\lambda = O(1) \Rightarrow \theta_z = O(1)$ and $\lambda \to 0 \Rightarrow \theta_z \gg O(1)$ at $z = z_0$. To do this we require items (i)–(v), below, each of which are straightforward to show:

(i)

$$\lim_{z\to 0}\{G_{zzz}\} = 0, \forall\lambda. \tag{B.1}$$

(ii) Near $z = 1$,

$$\theta_z = C_1 \exp(\mathscr{E})\{1 + (\mathscr{D} - \mathscr{E})(z - 1)\} + O((z - 1)^2), \tag{B.2}$$

where

$$z_0 = \frac{\mathscr{E}}{\mathscr{D}}, \qquad \mathscr{D} = \frac{\gamma_{2a}}{\lambda}, \qquad \mathscr{E} = \frac{\gamma_{2a} + 3\lambda - w_E}{\lambda}. \tag{B.3}$$

(iii) Near $z = z_0$,

$$\theta_z = C_1 \left(\frac{\mathscr{E}}{\mathscr{D}}\right)^{\mathscr{D}} \exp(\mathscr{D}) \left\{1 + \frac{\mathscr{D}^3}{2\mathscr{E}^2}\left(z - \frac{\mathscr{E}}{\mathscr{D}}\right)^2\right\} + O\left(\left(z - \frac{\mathscr{E}}{\mathscr{D}}\right)^3\right), \tag{B.4}$$

(iv) G_{zzz} has a single local extremum, at $z = z_0$ say, and two points of inflexion. For physical solutions the extremum should be maximum in the interval $z \in (0, 1)$. Hence we require

$$C_1 > 0, \qquad 0 < \frac{\gamma_{2a} + 3\lambda - w_E}{\gamma_{2a}} < 1. \tag{B.5}$$

(v)

$$\int_0^1 G_{zzz}\, dz = \theta_{\text{surf}} - \theta_{\text{bot}}, \tag{B.6}$$

which is independent of λ.

That $\lambda = O(1) \Rightarrow \theta_z = O(1)$ follows immediately from (i), (ii), (iii) and (iv). To see that $\lambda \to 0 \Rightarrow \theta_z \gg O(1)$, it is enough to note the following corollaries to (ii) and (iii): if $\mathscr{E} < 0$ (and therefore from (B.5), $\mathscr{D} < 0$), then

$$\lim_{\lambda \to 0} \{\theta_z(1)\} = 0;$$

and near $z = z_0$, G_{zzz} approximates a parabola, which narrows as λ decreases in magnitude. (The conditions $\mathscr{E} < 0$ and (B.5) are necessary for physical solutions.) In other words, we have a graph, under which is a constant area, both ends of which go to zero, which *does* have the shape indicated by Figure 4, and the maximum is narrowing. Hence the maximum must increase as $\lambda \to 0$. We have therefore shown that $O(\theta_z)$ increases without bound as $\lambda \to 0$ — a front forms! (Our "proof" is not as straightforward as we would like! It would be enought to show that $\lim_{\lambda \to 0} \{C_1(\lambda)\theta_z(z_0; \lambda)\} = \infty$, but as we have mentioned, the computation of $C_1(\lambda)$ appears intractable. One *can* show that $\lim_{\lambda \to 0} \{\theta_z(z_0)/\theta_z(1)\} = \infty$, provided $\gamma_{2a} \ln z_0 + w_E > 0$, but this shows only that $\theta_z(z_0)$ remains finite.)

APPENDIX C

In this section we derive the results quoted in the example considered in Section 4. Recall that we consider a simple case in which we have constant Ekman pumping and have chosen a particular, simple form for $\phi(y)$ (cf. (4.1b) and (4.17b)). We compute $G_0(\xi)$, $G_1(\xi)$ and $G_2(\xi)$ for the surface boundary layer and the ocean interior, in turn:

Surface Boundary Layer

It is convenient to introduce

$$H(\xi) = G_2^S(\xi) + G_1^S(\xi) + G_0^S(\xi), \tag{C.1}$$

then

$$w_E = G^S_{2,\xi} + G^S_{1,\xi} + G^S_{0,\xi} = H_\xi, \tag{C.2}$$

and integrating we obtain

$$H(\xi) = w_{E0}\xi + h_0 \tag{C.3}$$

and eliminating $G^S_1(\xi)$ in favor of $H(\xi)$ in (4.9) we find

$$[6g^S_3 - \gamma^S_2 + 2G^S_2(\xi)]G^S_{0,\xi} - 2G^S_{2,\xi}G^S_0(\xi) = \hat{k}_1, \tag{C.4i}$$

where $\hat{k}_1$ is defined by

$$\hat{k}_1 = (2g^S_{20} - \gamma^S_2)(w_{E0} - \hat{k}_2) - 2\hat{k}_2(\lambda_1^{-1}\lambda^S_2 + h_0 - g^S_{20}), \tag{C.4ii}$$

which is trivially integrable to obtain

$$G^S_0(\xi) = [6g^S_3 - \gamma^S_2 + 2G^S_2(\xi)]g^S_{00} - \frac{\hat{k}_1}{2\hat{k}_2}, \tag{C.5}$$

where g^S_{00} is a constant of integration.

We have now completely determined out solution in the Seasonal Thermocline. Collecting results we find,

$$M^S(x,y,z) = (\lambda_1 y)^{-1}[g^S_3 z^3 + z^2 G^S_2(\xi) + zG^S_1(\xi) + G^S_0(\xi)] + \left(\lambda^S_2 - \frac{\gamma^S_2 z}{2}\right)\frac{z}{\lambda_1 y} + A^S z^2, \tag{C.6a}$$

where

$$1 - \gamma^S_2\lambda^S_2 \neq 0, \qquad \hat{k}_2 \neq 0, \tag{C.6b}$$

$G^S_2(\xi)$ is given by (4.8) and is related to θ_{surf} by (4.10), $G^S_0(\xi)$ by (C.5) and

$$G^S_1(\xi) = (w_{E0} - \hat{k}_2 - 2g^S_{00}\hat{k}_2)\xi - g^S_{00}(6g^S_3 - \gamma^S_2 + 2g^S_{20}) + h_0 - g^S_{20} + \frac{\hat{k}_1}{2\hat{k}_2}. \tag{C.7}$$

Ocean Interior

To satisfy the condition on w at the interface (cf. (4.12)) we require

$$z_i^2 G^S_{2,\xi} + z_i G^S_{1,\xi} + G^S_{0,\xi} = z_i^2 G^I_{2,\xi} + z_i G^I_{1,\xi} \tag{C.8}$$

and integrating this and (4.6b) we obtain, respectively,

$$z_i^2 G^S_2 + z_i G^S_1 + G^S_0 = z_i^2 G^I_2 + z_i G^I_1 + \gamma^I_{20}, \tag{C.9a}$$

$$G^I_1 = g^I_{10}(2G^I_2(\xi) - \gamma^I_2) - \frac{\lambda^I_2}{\lambda_1}, \tag{C.9b}$$

where γ_{20}^I and g_{10}^I are constants of integration. Eqs. (C.9) are an exactly-determined algebraic system for $G_1^I(\xi)$ and $G_2^I(\xi)$, and have solution

$$G_2^I(\xi) = \frac{\mathcal{G}^S(\xi) + \hat{g}_0^I}{z_i(z_i + 2g_{10}^I)}, \tag{C.10a}$$

$$G_1^I(\xi) = \frac{2g_{10}^I(\mathcal{G}^S(\xi) + \hat{g}_0^I)}{z_i(z_i + 2g_{10}^I)} - \gamma_2^I(g_{10}^I + \lambda_2), \tag{C.10b}$$

where

$$\mathcal{G}^S = z_i^2 G_2^S(\xi) + z_i G_1^S(\xi) + G_0^S(\xi), \tag{C.10i}$$

$$\hat{g}_0^I = g_{20}^I - g_0^I + \left(\gamma_2^I + \frac{\lambda_2^I}{\lambda_1}\right) z_i. \tag{C.10ii}$$

(We assume that $z_i + 2g_{10}^I \neq 0$ as the singular case does not yield physical solutions.)

To ensure that θ is continuous across the interface (cf. 4.13) we require

$$(3z_i g_3^S + 2g_{20}^I - 3z_i g_3^I) = 2(z_i^2 g_{20}^S + z_i(w_E - \hat{k}_2 - 2g_{00}^S \hat{k}_2) + 2g_{00}^S g_{20}^S. \tag{C.11}$$

Finally we consider the eastern boundary condition (cf. (2.6)). This becomes

$$\int_{z=0}^{z=z_i} \int_{y=0}^{y=1} u^I(x = 1, y, z)\, dydz + \int_{z=z_i}^{z=1} \int_{y=0}^{y=1} u^S(x = 1, y, z)\, dydz = 0 \tag{C.12}$$

and determines one of the parameters in our solution in terms of the others.

We have now completely determined our solution in the Main Thermocline; collecting results we find

$$M^I(x, y, z) = (\lambda_1 y)^{-1}\{g_3^I z^3 + z^2 G_2^I(\xi) + z G_1^I(\xi) + g_0^I + [\lambda_2^I - \tfrac{1}{2}\gamma_2^I z]z\} + A^I z^2, \tag{C.13a}$$

where

$$z_i \neq 0, \qquad z_i + 2g_{10}^I \neq 0, \tag{C.13b}$$

and $G_1^I(\xi)$ and $G_2^I(\xi)$ are given by (C.10).

REFERENCES

Abramowitz, M. and I. A. Stegun. 1972. Handbook of Mathematical Functions, 10th edition, Dover, New York.

Clarkson, P. A. and M. D. Kruskal. 1989. New similarity solutions of the Boussinesq equation. J. Math. Phys., *30,* 2201–2213.

Gent, P. R., J. Willebrand, T. J. McDougall and J. C. McWilliams. 1995. Parameterizing eddy-induced tracer transports in ocean circulation models. J. Phys. Oceanogr., *25,* 463–474.

Hood, S. 1996. New similarity solutions of the thermocline equations with vertical variation of diffusion. J. Mar. Res., *54,* 187–209.

Huang, R. X. 1988. On boundary value problems of the ideal-fluid thermocline. J. Phys. Oceanogr., *18,* 619–641.

Luyten, J. R., J. Pedlosky and H. Stommel. 1983. The ventilated thermocline. J. Phys. Oceanogr., *13,* 292–309.

Marshall, J. C. and A. J. G. Nurser. 1991. A continuously, stratified thermocline model incorporating a mixed layer of variable depth and density. J. Phys. Oceanogr., *21,* 1780–1792.

Nurser, A. J. G. and J. C. Marshall. 1991. On the relationship between subduction rates and diabatic forcing of the mixed layer. J. Phys. Oceanogr., *21,* 1793–1802.

Pedlosky, J. 1986. Thermocline theories, *in* General Circulation of the Ocean, H. D. I. Arbarbanal and W. R. Young ed., Springer Verlag, New York.

Pedlosky, J., W. Smith and J. R. Luyten. 1984. On the dynamics of the coupled mixed-layer-thermocline system and the determination of the oceanic surface density. J. Phys. Oceanogr., *40,* 1159–1171.

Rhines, P. B. 1986. Vorticity dynamics of the oceanic general circulation. Ann. Rev. Fluid Mech., *18,* 433–497.

Rhines, P. B. and W. R. Young. 1982. A theory of wind-driven circulation. I: mid-ocean gyres. J. Mar. Res., *40*(suppl.), 559–595.

Robinson, A. R. and H. Stommel. 1959. The ocean thermocline and the associated thermohaline circulation. Tellus, *11,* 295–308.

Salmon, R. 1990. The thermocline as an "internal boundary layer." J. Mar. Res., *48,* 437–469.

Salmon, R. and R. Hollerbach. 1991. Similarity solutions of the thermocline equations. J. Mar. Res., *49,* 249–280.

Samelson, R. M. and G. K. Vallis. 1996a. Planetary geostrophic equations for large-scale ocean modelling. J. Phys. Oceanogr., (submitted).

—— 1996b. Large-scale circulation with small diapycnal diffusion: the two-thermocline limit. J. Mar. Res., (submitted)

Welander, P. 1971. Some exact solutions to the equations describing an ideal-fluid thermocline. J. Mar. Res., *21,* 60–68.

—— 1959. An advective model of the ocean thermocline. Tellus, *11,* 309–318.

Williams, R. G. 1991. The role of the mixed layer in setting the potential vorticity of the main thermocline. J. Phys. Oceanogr., *21,* 1803–1814.

—— 1989. Influence of air-sea interaction on the ventilated thermocline. J. Phys. Oceanogr., *19,* 1255–1267.

Woods, J. D. 1984. The upper ocean and air-sea interaction in global climate, *in* The Global Climate, J. T. Houghton, ed., Cambridge University Press, 141–187.

Received: *21 March, 1995;* revised: *14 September 1995.*